Cubic-symmetry acoustic metamaterials with roton-like dispersion relations

Ke Wang[1,2†], Yi Chen[2,3], Muamer Kadic[3,4], Changguo Wang[1], and Martin Wegener[2,3]

[1]National Key Laboratory of Science and Technology for National Defence on Advanced Composites in Special Environments, Harbin Institute of Technology, Harbin 150001, P. R. China.

[2]Institute of Applied Physics, Karlsruhe Institute of Technology (KIT), Karlsruhe 76128, Germany.

[3]Institute of Nanotechnology, Karlsruhe Institute of Technology (KIT), Karlsruhe 76128, Germany.

[4]Institut FEMTO-ST, UMR 6174, CNRS, Université de Franche-Comté, Besançon 25030, France.

E-mail: (ke.wang2@partner.kit.edu (K.W.))

Abstract: In our previous work, we have shown that nonlocal interactions in acoustic metamaterials can lead to highly unusual roton-like dispersion relations exhibiting a minimum of frequency versus wavenumber similar to that of superfluid Helium-4. However, this behavior was limited to only one or two propagation directions of sound. Here, we design a three-dimensional cubic-symmetry airborne acoustic metamaterial with nonlocal interactions along three orthogonal directions. By using numerical finite-element calculations, we show that the metamaterial supports roton-like behavior along all three orthogonal directions, but the behavior is far from isotropic. We compare these calculations with a simplified semi-analytical model, leading to good overall agreement. Corresponding experiments appear in reach, but are demanding due to the required dense and complex three-dimensional network of acoustic channels that connect compartments of air.

Keywords: acoustic metamaterials, dispersion bands, roton-like dispersions, cubic symmetry

1. Introduction

The dispersion relation of sound waves in most ordinary acoustic media such as, e.g., air or water is given by a constant speed of sound that connects the frequency and the wavenumber of the wave[1, 2]. To improve the possibilities of controlling and steering acoustic waves, efforts have been undertaken to design airborne or waterborne metamaterials with stop bands arising from Bragg reflections[3, 4] or adjustable positive phase velocity by geometrical detours[5, 6] or with negative phase velocity with respect to group velocity by exploiting local resonances[7, 8]. More recently[9-12], with roots going back all the way to Brillouin[13], we have used nonlocal interactions in airborne acoustic metamaterials as a means to obtain dispersion relations of the lowest branch that resemble that of sound waves in superfluid helium. There, the dispersion relation starts with frequency being proportional to wavenumber. For larger wavenumbers, frequency exhibits a maximum, followed by a region of negative slope and a minimum, which is referred to as the roton[14-23]. The region of negative slope corresponds to backward waves over a large relative bandwidth, i.e., to a situation for which the phase velocity is opposite to the group velocity. For sufficiently small damping, the group velocity vector points in the same direction as the energy flow.

In our previous work, we were able to design three-dimensional acoustic-metamaterial architectures for which roton-like dispersion behavior becomes possible for one[9] or two[11] orthogonal propagation directions of sound. These metamaterials were composed of compartments of air connected by air channels supporting the local and nonlocal interactions among the compartments. Here, we extend this idea to a three-dimensional cubic-symmetry acoustic metamaterial for which the unusual roton-like behavior occurs for all three principal cubic directions. While this extension is straightforward conceptually, the design challenge has been a geometric one. The many channels mediating the local and nonlocal interactions in three dimensions have to be arranged such that no intersections occur, while maintaining sufficiently large channel cross sections to allow for sufficiently strong nonlocal interactions.

2. Metamaterial design

Figure 1**a** depicts a unit cell of designed acoustic metamaterial for airborne sound. The light-yellow cuboid located in the center of the unit cell is a compartment for air. The light-yellow cylinders and the light-blue cylinders represent air channels for mediating nearest-neighboring (local) interactions and third-nearest-neighboring (nonlocal) interactions, respectively. In contrast to a single channel for coupling pressures in two neighboring compartments, that are four channels between two third-nearest-neighboring compartments (one is highlighted in Fig. 1**b**) in order to main the cubic-symmetry. This design drastically increases the number of channels in the metamaterial and significantly complicates the geometry[11]. Therefore, we specially design and arrange these channels in space (cf. detours of light-blue channels in Fig. 1**a**) to avoid unwanted intersections between them. Light-yellow channels and light-blue channels have radius R_1 and R_3, respectively. Once the length of the channels is fixed, relative strength between local interactions and nonlocal interactions can be tailored via these two

radii[11]. Sufficiently large ratios R_3/R_1 leads to the wanted roton-like dispersion relations, as we will demonstrate below.

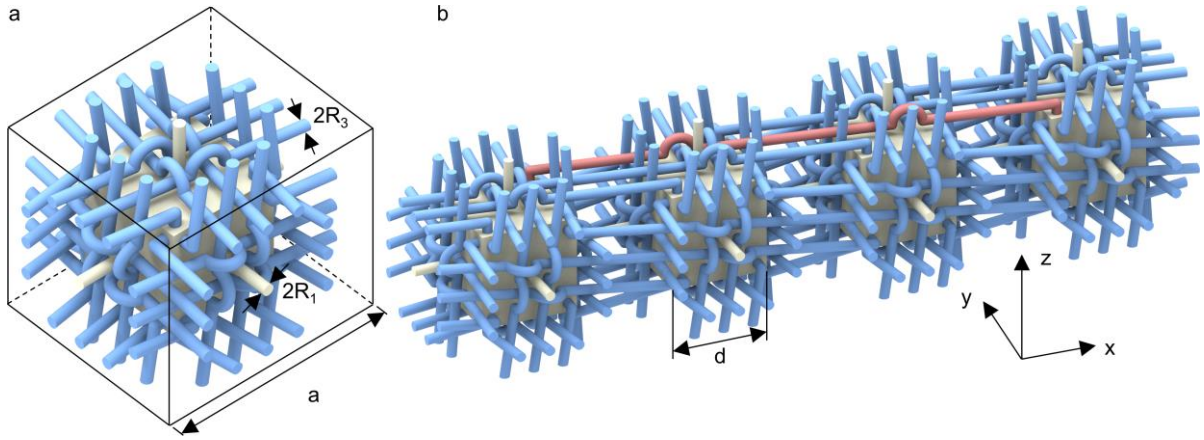

Fig. 1. Illustration of the designed cubic-symmetry acoustic metamaterial. **a** One metamaterial unit cell with lattice constant a. An infinite bulk metamaterial is obtained by replicating the cubic unit cell in three dimensional space according to a simple-cubic lattice. The light-yellow cuboid represents an air compartment. Pressures in two neighboring compartments and two third-nearest-neighboring compartments are coupled by air channels in light-yellow and light-blue, respectively. **b** An array of four unit cells along x-directions. One channel connecting the first cuboid compartment to the last along the array is heighted in red. We choose $d/a = 0.5$ for our below calculations.

3. Numerical and theoretical modeling

3.1 Finite element calculations

We numerically solve dispersion bands for the designed acoustic metamaterial by using the commercial software COMSOL Multiphysics with the Acoustic Pressure Module. Specifically, the following governing equation for linear acoustics is solved[1]

$$\nabla \cdot \left(\nabla \tilde{P}_{\mathbf{k},n}(\mathbf{r})\right) = -\frac{\omega_n^2(\mathbf{k})}{v_{\text{air}}^2}\tilde{P}_{\mathbf{k},n}(\mathbf{r}), \tag{1}$$

for finding the eigenfrequencies $\omega_n(\mathbf{k})$, with band index n and Bloch wavevector $\mathbf{k}$, and the corresponding eigenmodes $\tilde{P}_{\mathbf{k},n}(\mathbf{r})$. Here, $\tilde{P}_{\mathbf{k},n}(\mathbf{r})$ should be understood as the pressure variation relative to a constant background atmospheric pressure. v_{air} represents the speed of sound in air and is chosen as $v_{\text{air}} = 340\ \text{m/s}$ for the FEM simulations and the below simplified theoretical treatment. We apply Bloch periodic boundary conditions to the six surfaces of the cubic metamaterial unit cell (cf. Fig. 1). All other boundaries are treated to be sound rigid[1]. The eigenfrequencies and eigenmodes are obtained by using the MUMPS solver in Comsol Multiphysics.

3.2 Transmission line model

Next, we adopt a transmission line approach similar to our previous work[11] and theoretically derive acoustic dispersion bands of our designed metamaterial. Transmission line theory is

generally applicable to the low-frequency range, where the corresponding wavelength is much larger than cavities and diameters of channels in the acoustic metamaterial. These conditions are well satisfied for the lowest bands as demonstrated by FEM calculations and theory later. Below, we provide the main steps for the analysis.

We consider an infinite bulk metamaterial composed of the unit cell shown in Fig. 1(a). For brevity, we number each lattice site by three integers (m,n,l) with $m,n,l = 0,\pm1,\pm2$ .... . At low frequency range, acoustic pressure fields in each cuboid compartment can be assumed to be uniform[11]. Following the Floquet-Bloch wave theorem[2], we denote the acoustic pressure in the cuboid compartment at lattice site (m,n,l) to be $P_{mnl} = \tilde{P}\exp(\mathrm{i}(k_x ma + k_y na + k_z la - \omega t))$, with $\tilde{P}$ being a constant prefactor, ω being the angular frequency, k_x, k_y, k_z being three components of the Bloch wavevector $\mathbf{k} = (k_x, k_y, k_z)$, and the imaginary unit i. On this basis, we address wave propagation in the channels in Fig. 1.

We first consider wave propagations in the light-yellow channels that connect two neighboring compartments. As one example, we analyze the channel that connects the compartment at site (m,n,l) to its immediate neighbor along x-direction at site $(m+1,n,l)$. Within the low-frequency range, only the zeroth guided mode, of which pressure fields inside the channel are uniform on the cross section, is a propagation mode in the tube while other guided modes are evanescent[1]. We obtain pressure fields inside the channel as a superposition of a forward zeroth guided mode, from the cuboid at site (m,n,l) to that at site $(m+1,n,l)$, and a corresponding backward mode[24]

$$P(s) = \left(A^+ \exp\left(\mathrm{i}\frac{\omega}{v_{\mathrm{air}}}s\right) + A^- \exp\left(-\mathrm{i}\frac{\omega}{v_{\mathrm{air}}}s\right)\right)\exp(-\mathrm{i}\omega t). \tag{2}$$

Herein, s indicates the distance along the central axis of the channel with $s = 0$ being one end of the channel, where it connects to the cuboid at site (m,n,l). Then, $s = L_1$, with $L_1 = a - d$ being the channel length, representing the other end. A^+ and A^- are two unknown amplitude coefficients. The corresponding particle velocity is derived as

$$v(s) = \frac{1}{\mathrm{i}\omega\rho_{\mathrm{air}}}\frac{\partial P}{\partial s} = \frac{1}{\rho_0 v_{\mathrm{air}}}\left(A^+ \exp\left(\mathrm{i}\frac{\omega}{v_{\mathrm{air}}}s\right) - A^- \exp\left(-\mathrm{i}\frac{\omega}{v_{\mathrm{air}}}s\right)\right)\exp(-\mathrm{i}\omega t), \tag{3}$$

with ρ_{air} representing average air density. Now, we apply continuity conditions at both ends of the channel, i.e., acoustic pressures must be the same as that in the corresponding cuboids[24]

$$P(0) = \tilde{P}\exp\left(\mathrm{i}k_x ma + \mathrm{i}k_y na + \mathrm{i}k_z la - \mathrm{i}\omega t\right), \tag{4}$$

$$P(L_1) = \tilde{P}\exp\left(\mathrm{i}k_x (m+1)a + \mathrm{i}k_y na + \mathrm{i}k_z la - \mathrm{i}\omega t\right), \tag{5}$$

Substituting Eq. (2) into Eqs. (4) and (5) yields the two amplitude coefficients, A^+ and A^-,

$$A^+ = \frac{\tilde{P}}{2\mathrm{i}}\exp\left(\mathrm{i}k_x ma + \mathrm{i}k_y na + \mathrm{i}k_z la\right)\csc\left(\frac{\omega L_1}{v_{\mathrm{air}}}\right)\left(\exp(\mathrm{i}k_x a) - \exp(-\mathrm{i}\frac{\omega L_1}{v_{\mathrm{air}}})\right), \tag{6}$$

$$A^- = \frac{\tilde{P}}{2\mathrm{i}}\exp\left(\mathrm{i}k_x ma + \mathrm{i}k_y na + \mathrm{i}k_z la\right)\csc\left(\frac{\omega L_1}{v_{\mathrm{air}}}\right)\left(-\exp(\mathrm{i}k_x a) + \exp(\mathrm{i}\frac{\omega L_1}{v_{\mathrm{air}}})\right). \tag{7}$$

The particle velocity in Eq. (3) can be simplified to

$$v(s) = \frac{\mathrm{i}\, P_{mnl}}{\rho_{\mathrm{air}} v_{\mathrm{air}}} \csc\left(\frac{\omega L_1}{v_{\mathrm{air}}}\right)\left(\cos\left(\frac{\omega s - \omega L_1}{v_{\mathrm{air}}}\right) - \cos\left(\frac{\omega s}{v_{\mathrm{air}}}\right)\exp(\mathrm{i}k_x a)\right). \quad (8)$$

From this expression, the total air mass flowing out of the cuboid at lattice site (m, n, l) through the above channel is given by

$$Q_{m+1,n,l} = \rho_{\mathrm{air}} S_1 v(0) = \mathrm{i}\frac{S_1 P_{mnl}}{v_{\mathrm{air}}} \csc\left(\frac{\omega L_1}{v_{\mathrm{air}}}\right)\left(\cos\left(\frac{\omega L_1}{v_{\mathrm{air}}}\right) - \exp(\mathrm{i}k_x a)\right). \quad (9)$$

Herein, $S_1 = \pi R_1^2$ represents the cross section of the nearest-neighbor channel. Likewise, the air mass flow out the cuboid compartment at lattice site (m, n, l) through nearest-neighboring channels along the *y*-direction and *z*-direction to the compartment at lattice sites $(m, n+1, l)$ and $(m, n, l+1)$ are given by

$$Q_{m,n+1,l} = \mathrm{i}\frac{S_1 P_{mnl}}{v_{\mathrm{air}}} \csc\left(\frac{\omega L_1}{v_{\mathrm{air}}}\right)\left(\cos\left(\frac{\omega L_1}{v_{\mathrm{air}}}\right) - \exp\left(\mathrm{i}k_y a\right)\right), \quad (10)$$

$$Q_{m,n,l+1} = \mathrm{i}\frac{S_1 P_{mnl}}{v_{\mathrm{air}}} \csc\left(\frac{\omega L_1}{v_{\mathrm{air}}}\right)\left(\cos\left(\frac{\omega L_1}{v_{\mathrm{air}}}\right) - \exp(\mathrm{i}k_z a)\right). \quad (11)$$

Apart from the channels connecting immediate neighboring compartments, we further need to consider wave propagations in channels between third-nearest-neighboring compartments. The analysis is similar. The total air mass flow through *each* channel from the compartment at lattice site (m, n, l) to the compartment at lattice sites $(m+3, n, l)$, $(m, n+3, l)$ and $(m, n, l+3)$ are, respectively,

$$Q_{m+3,n,l} = \mathrm{i}\frac{S_3 P_{mnl}}{v_{\mathrm{air}}} \csc\left(\frac{\omega L_3}{v_{\mathrm{air}}}\right)\left(\cos\left(\frac{\omega L_3}{v_{\mathrm{air}}}\right) - \exp(3\mathrm{i}k_x a)\right), \quad (12)$$

$$Q_{m,n+3,l} = \mathrm{i}\frac{S_3 P_{mnl}}{v_{\mathrm{air}}} \csc\left(\frac{\omega L_3}{v_{\mathrm{air}}}\right)\left(\cos\left(\frac{\omega L_3}{v_{\mathrm{air}}}\right) - \exp\left(3\mathrm{i}k_y a\right)\right), \quad (13)$$

$$Q_{m,n,l+3} = \mathrm{i}\frac{S_3 P_{mnl}}{v_{\mathrm{air}}} \csc\left(\frac{\omega L_3}{v_{\mathrm{air}}}\right)\left(\cos\left(\frac{\omega L_3}{v_{\mathrm{air}}}\right) - \exp(3\mathrm{i}k_z a)\right), \quad (14)$$

with $S_3 = \pi R_3^2$ being the cross section area of the nonlocal channel and L_3 representing their length. The expression of L_3 is rather lengthy and is not given here. For the compartment at lattice site (m, n, l), the conservation law for air mass requires[24]

$$\mathrm{i}\frac{\omega}{v_{\mathrm{air}}^2} V_{\mathrm{c}} \tilde{P}_{mnl} = \left(Q_{m+1,n,l} - Q_{m-1,n,l} + Q_{m,n+1,l} - Q_{m,n-1,l} + Q_{m,n,l+1} - Q_{m,n,l-1}\right) + 4\left(Q_{m+3,n,l} - Q_{m-3,n,l} + Q_{m,n+3,l} - Q_{m,n-3,l} + Q_{m,n,l+3} - Q_{m,n,l-3}\right). \quad (15)$$

$V_c = d^3$ represents the compartment volume. $Q_{m-1,n,l}$ is the mass flow in through the channel that connects the cuboid at site $(m-1, n, l)$ and to that at site (m, n, l) and $Q_{m-3,n,l}$ is the mass flow in through each of the four channels between the two cuboids at sites (m, n, l) and $(m-3, n, l)$. Other symbols can be understood in analogy. We remark here that the factor 4 in front of the second term on the right-hand side of Eq. (15) is due to four nonlocal channels between two third-nearest-neighboring compartments.

After substituting the mass flow formula into Eq. (15) and some mathematical simplifications, we derive an implicit expression for the acoustic dispersion bands of the designed cubic-symmetry acoustic metamaterial

$$\frac{\omega}{v_{\text{air}}}V_c = S_1 \csc\left(\frac{\omega L_1}{v_{\text{air}}}\right)\left(6\cos\left(\frac{\omega L_1}{v_{\text{air}}}\right) - 2\cos(k_x a) - 2\cos(k_y a) - 2\cos(k_z a)\right) + 4S_3 \csc\left(\frac{\omega L_3}{v_{\text{air}}}\right)\left(6\cos\left(\frac{\omega L_3}{v_{\text{air}}}\right) - 2\cos(3k_x a) - 2\cos(3k_y a) - 2\cos(3k_z a)\right). \quad (16)$$

This equation does not provide a closed expression for the angular frequency $\omega = \omega(k_x, k_y, k_z)$., However, (16) can be easily solved numerically for a given Bloch wavevector $\mathbf{k} = (k_x, k_y, k_z)$. Note that for any given $\mathbf{k}$, multiple solutions for ω can be derived from the implicit formula Eq. (15). These solutions correspond to different bands. In the long wavelength limit, i.e., $k_x a/\pi \ll 1, k_y a/\pi \ll 1, k_z a/\pi \ll 1$, and $\omega \ll v_{\text{air}}\pi/L_3$, we can turn Eq. (16) into an explicit expression for the angular frequency ω by Tayler expansion

$$\omega \approx \sqrt{\frac{S_1/L_1 + 36S_3/L_3}{V_c + 3L_1S_1 + 12L_3S_3}}\, v_{\text{air}} a \sqrt{k_x^2 + k_y^2 + k_z^2}. \quad (17)$$

The direction independent linear dispersion relation Eq. (17) indicates an isotropic behavior of our metamaterial in the long-wavelength limit, as expected from the cubic-symmetry. In the following Figs. 2-4, we show results for the transmission-line model as well as FEM calculations. Both results are in good agreement not just for the lowest bands but also for higher bands along arbitrary wave-propagation directions.

4. Comparison between the semi-analytical model and FEM calculations

First, we study the acoustic bands along the principal cubic direction. In Fig. 2, we plot the lowest band for a set of three different radii, i.e., $R_3/a = 0.01$, $R_3/a = 0.02$, and $R_3/a = 0.03$. The lattice constant and the channel radius for local interactions are fixed to $a = 10$ cm and $R_1/a = 0.02$. The theoretical results are denoted by dots and the FEM calculations are shown by solid curves to allow for direct comparisons. Higher bands occur above 600 Hz and are not shown in Fig. 2. From a small ratio of $R_3/a = 0.01$ for the nonlocal channels to a larger one of $R_3/a = 0.02$, the dispersion band develops a roton-like behavior with a local minimum around $k_z a/\pi \approx 0.65$. For even larger values of $R_3/a = 0.03$, we observe an even more pronounced roton-like minimum with an even smaller $\omega(k_z a/\pi \approx 0.65)$.

In Figs. 3 and 4, we start from the same set of geometrical parameters. Further increasing the radius of the nonlocal channels leads to an unwanted geometrical overlap between them. In the frequency range between 90 Hz and 160 Hz, each frequency has three eigenmodes with different wavenumbers, a characteristic feature of roton-like bands[9]. If a wave packet impinges from an ordinary medium (e.g., air) onto such a metamaterial, three refracted wave packets would emerge with different refraction angles[11]. The one with negative group velocity, $\mathrm{d}\omega/\mathrm{d}k < 0$, leads to broadband negative refraction. In local metamaterials, the regime of negative refraction is usually limited to a narrow frequency range[25, 26]. As can be seen from Figs. 3 and 4, results of the semi-analytical model are nearly identical to the FEM calculations in the plotted frequency range below 200 Hz, of which the corresponding wavelength in air is

around 20 times larger than the lattice constant. The analytical model also shows high accuracy for higher bands as well as for general wave directions other than the principal cubic directions. Figure 3 exhibits the complete bands through sweeping the Bloch wavevector along the usual tour (Fig. 3(a)) for cubic crystals in reciprocal space. The relatively long nonlocal channels in the metamaterial support local resonances at low frequency, with negligible pressures in compartments. Therefore, the wavelength is around twice of the channel length and the corresponding frequencies can be estimated as $v_{\text{air}}/(2L_3) = 585$ Hz. The multiple nearly flat bands around 600 Hz are due to these local modes.

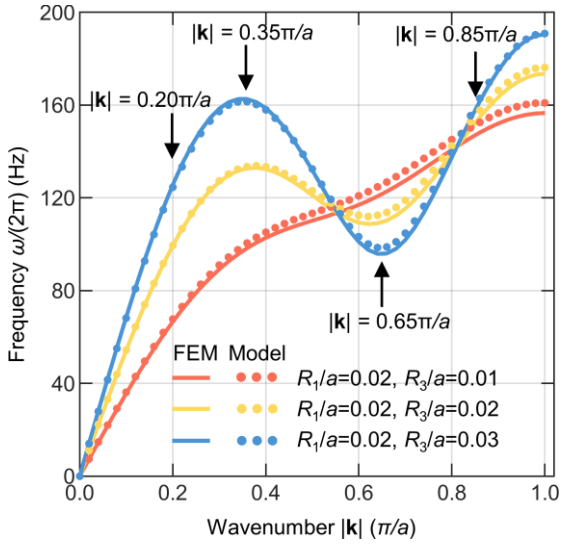

Fig. 2. Roton-like dispersion relations along the equivalent principal cubic directions. We choose a lattice constant $a = 10$ cm and fix the normalized radius of the nearest-neighbor channels to $R_1/a = 0.02$. Dispersion bands are plotted for three different radii of nonlocal channels, $R_3/a = 0.01$, $R_3/a = 0.02$, and $R_3/a = 0.03$. Higher branches occur slightly below 600 Hz (not depicted here, see Fig. 3). Results for the analytical model and FEM calculations are represented by dots and solid curves, respectively. Four arrows indicate the wavenumbers considered in Fig. 4.

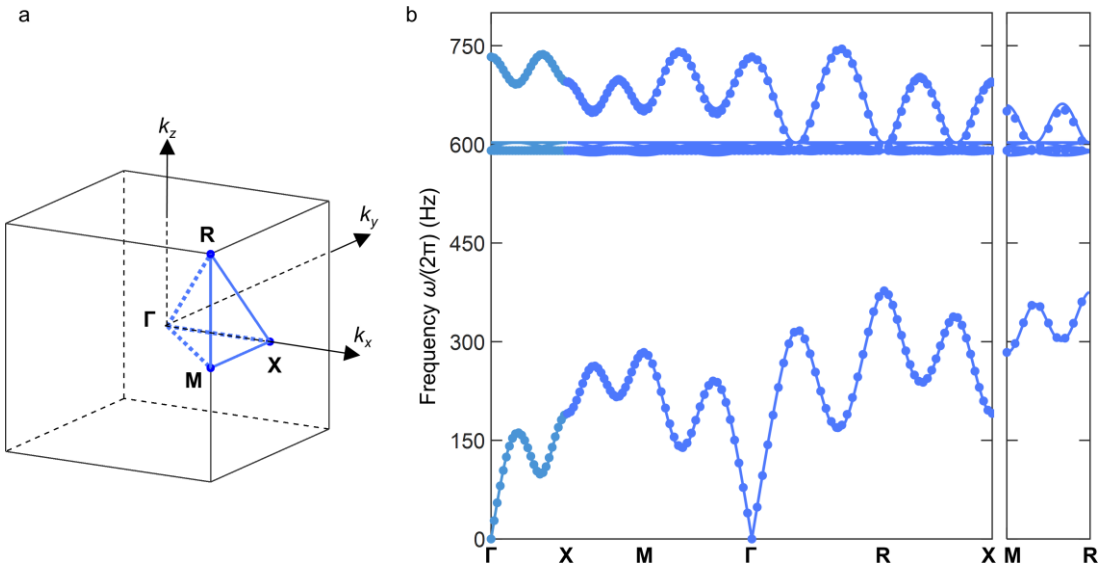

Fig. 3. Acoustic bands along high-symmetry directions of the designed cubic-symmetry metamaterial. **a** Sketch of the first Brillouin zone. We sweep the Bloch wavevector **k** along the blue lines, which mark edges of an irreducible zone in reciprocal space. **b** First and higher

dispersion bands along the marked edges in **a**. As in Fig. 2, calculated bands are represented by dots and FEM results by solid curves. The geometrical parameters $a = 10$ cm, $R_1/a = 0.02$, and $R_3/a = 0.03$ are used.

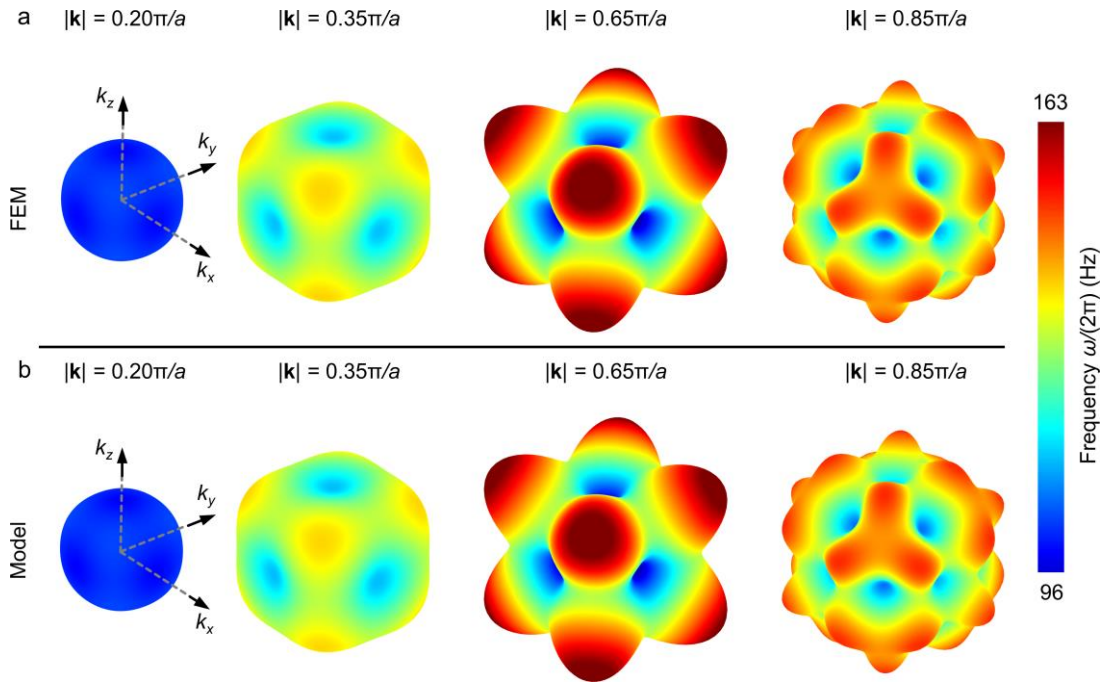

Fig. 4. Plots of the first eigenfrequency at fixed length of the Bloch wavevector $|\mathbf{k}|$ but different wavevector directions. **a** Results for FEM simulations. From left to right, we choose the length of the wavevector $|\mathbf{k}| = 0.20\,\pi/a$, $|\mathbf{k}| = 0.35\,\pi/a$, $|\mathbf{k}| = 0.65\,\pi/a$, and $|\mathbf{k}| = 0.85\,\pi/a$ (cf. also the four arrows in Fig. 2). The frequencies for different directions are encoded by the distances of points on the surface to the origin as well by as false-color scale. **b** Same as in **a**, but for the semi-analytical model. The geometrical parameters are the same as in Fig. 3.

It is also interesting to compare wave propagation along different directions in the cubic-symmetry metamaterial. In Fig. 4, we illustrate the direction dependences of the eigenfrequencies of the first band at a fixed length of the wavevector $|\mathbf{k}|$, but for different directions. From left to right, we have chosen the four different values: $|\mathbf{k}| = 0.20\,\pi/a$, $0.35\,\pi/a$, $0.65\,\pi/a$, and $0.85\,\pi/a$ (also cf. arrows in Fig. 2). Panel **a** shows FEM calculations and panel **b** the semi-analytical model. For each point on these surface plots, the distance to the origin is a measure for the eigenfrequency for wave propagating in that direction. In this representation, spherical surfaces represent isotropic behavior. For a relatively small wavenumber of $|\mathbf{k}| = 0.20\,\pi/a$, the plot is indeed close to spherical, as theoretically predicated from Eq. (17). The surface generally grows outward with increasing wavenumber and the anisotropy becomes very obvious at finite wavenumbers. At the wavenumber $|\mathbf{k}| = 0.35\,\pi/a$, the surface along the principal cubic directions develops into a nearly flat surface. For an even larger wavenumber, the flat parts start to decrease towards the origin, due to occurrences of a negative group velocity (cf. Fig. 2), indicating a transition from nearly isotropic behavior of the metamaterial to a highly anisotropic one. This behavior is directly related to the spatial dispersion of our metamaterial which includes nonlocal interactions[27]. In phononic crystals or metamaterials, similar transitions from isotropy to highly anisotropic behavior usually occur

close to the edges of Brillouin zone[4]. In contrast, here, spatial-dispersion effects are pronounced at much smaller wavenumbers, which is favorable for theoretical modeling by an effective continuum model. Our metamaterial may provide a suitable platform for studying spatial dispersion and nonlocal effects by effective medium theory[27, 28]. Notches are most clearly observed at the roton minimum $|\mathbf{k}| = 0.65\ \pi/a$ and also emerge in the face-diagonal directions (right-most column) for wavenumbers $|\mathbf{k}| = 0.85\ \pi/a$ approaching the Brillouin zone edges.

5. Conclusion

Based on our previous acoustic metamaterials with nonlocal interactions, we have designed a cubic-symmetry acoustic metamaterial that supports roton-like acoustic bands along three principal cubic directions. We have theoretically derived corresponding dispersion relations for sound propagation by using transmission-line theory. The direct comparison with FEM calculations has validated the developed semi-analytical model, which predicts the behavior of the lowest acoustic branches along the principal cubic directions as well as other directions. Interesting spatial dispersion effects due to the pronounced nonlocality are observed in the metamaterial even for wavenumbers far from the Brillouin zone edge. The designed metamaterial may provide a platform for studying broadband negative refraction in three-dimensional space or serve as a metamaterial model with cubic-symmetry for investigating nonlocal effects and related spatial dispersions by using effective-medium continuum theory.

Acknowledgments

K.W. acknowledges support by the China Scholarship Council (CSC). This research has additionally been funded by the Deutsche Forschungsgemeinschaft (DFG, German Research Foundation) under Germany's Excellence Strategy via the Excellence Cluster “3D Matter Made to Order” (EXC-2082/1-390761711), which has also been supported by the Carl Zeiss Foundation through the “Carl-Zeiss-Foundation-Focus@HEiKA”, by the State of Baden-Württemberg, and by the Karlsruhe Institute of Technology (KIT). We further acknowledge support by the Helmholtz program “Materials Systems Engineering” (MSE). M.K. is grateful for support by the EIPHI Graduate School (contract ANR-17-EURE-0002). C.W. is grateful for support by the National Natural Science Foundation of China (contract 11872160).

Author contributions

K.W. and Y.C. performed the numerical simulations and theoretical derivations. K.W. and M.K. designed the metamaterials. Y.C. and M.W. wrote the first draft. C.W. and M.W. supervised the effort. All authors discussed the results and contributed to the writing and reviewing of the manuscript.

Conflict of interests

Authors declare that they have no competing interests.

Data and code availability

The data that support the plots within this paper and other findings of this study are available from the corresponding authors upon reasonable request and are published on the open access data repository of the Karlsruhe Institute of Technology [Enter repository].

References:

[1] Kinsler, L. E., Frey, A. R., Coppens, A. B., et al. Fundamentals of acoustics. New York: Wiley, 1999.

[2] Kittel, C. Introduction to solid state physics. New York: Wiley, 2005.

[3] Martínez-Sala, R., Sancho, J., Sánchez, J. V., et al: Sound attenuation by sculpture. Nature **378**, 241 (1995) 10.1038/378241a0.

[4] Deymier, P. A. Acoustic metamaterials and phononic crystals. New York: Springer, 2013.

[5] Liang, Z. X., Li, J.: Extreme acoustic metamaterial by coiling up space. Phys Rev Lett **108**, 114301 (2012) 10.1103/PhysRevLett.108.114301.

[6] Frenzel, T., David Brehm, J., Bückmann, T., et al: Three-dimensional labyrinthine acoustic metamaterials. Appl Phys Lett **103**, 61907 (2013) 10.1063/1.4817934.

[7] Kaina, N., Lemoult, F., Fink, M., et al: Negative refractive index and acoustic superlens from multiple scattering in single negative metamaterials. Nature **525**, 77 (2015) 10.1038/nature14678.

[8] Cummer, S. A., Christensen, J., Alù, A.: Controlling sound with acoustic metamaterials. Nat. Rev. Mater. **1**, 1 (2016) 10.1038/natrevmats.2016.1.

[9] Chen, Y., Kadic, M., Wegener, M.: Roton-like acoustical dispersion relations in 3D metamaterials. Nat. Commun. **12**, 3278 (2021) 10.1038/s41467-021-23574-2.

[10] Martínez, J. A. I., Groß, M. F., Chen, Y., et al: Experimental Observation of Roton-Like Dispersion Relations in Metamaterials. Sci. Adv. **7**, m2189 (2021) 10.1126/sciadv.abm218.

[11] Wang, K., Chen, Y., Kadic, M., et al: Nonlocal interaction engineering of 2D roton-like dispersion relations in acoustic and mechanical metamaterials. Commun. Mat. **3**, 1 (2022) 10.1038/s43246-022-00257-z.

[12] Chen, Y., Abouelatta, M. A. A., Wang, K., et al: Nonlocal cable-network metamaterials. submitted (2022)

[13] Brillouin, L. Wave propagation in periodic structures: electric filters and crystal lattices.

Dover publications, 1953.
[14] Landau, L.: Theory of the Superfluidity of Helium II. Phys. Rev. **60**, 356 (1941) 10.1103/PhysRev.60.356.
[15] Feynman, R. P.: Atomic theory of the two-fluid model of liquid helium. Phys. Rev. **94**, 262 (1954) 10.1103/PhysRev.94.262.
[16] Godfrin, H., Beauvois, K., Sultan, A., et al: Dispersion relation of Landau elementary excitations and thermodynamic properties of superfluid He 4. Phys. Rev. B **103**, 104516 (2021) 10.1103/PhysRevB.103.104516.
[17] Fleury, R.: Non-local oddities. Nat. Phys. **17**, 766 (2021) 10.1038/s41567-021-01281-5.
[18] Zhu, Z., Gao, Z., Gui-Geng, L., et al: Observation of multiple rotons and multidirectional roton-like dispersion relations in acoustic metamaterials. New J. Phys **24**, 123019 (2022) 10.1088/1367-2630/aca786.
[19] Iorio, L., De Ponti, J. M., Maspero, F., et al: Roton-like dispersion via polarisation change for elastic wave energy control in graded delay-lines. arXiv preprint arXiv:2211.09431 (2022)
[20] Cui, J., Yang, T., Niu, M., et al: Tunable roton-like dispersion relation with parametric excitations. Journal of Applied Mechanics **89**, 111005 (2022) 10.1115/1.4055545.
[21] Chaplain, G. J., Hooper, I. R., Hibbins, A. P., et al: Reconfigurable Elastic Metamaterials: Engineering Dispersion with Meccano^{TM}. arXiv preprint arXiv:2206.10487 (2022)
[22] Wu, Q., Shivashankar, P., Xu, X., et al: Engineering nonreciprocal wave dispersion in a nonlocal micropolar metabeam. J. Compos Mater 40562 (2022) 10.1177/002199832211405.
[23] Yang, L., Wang, L.: Gradient Continuum Model of Nonlocal Metamaterials with Long-range Interactions. Phys Scripta (2022) 10.1088/1402-4896/aca93e.
[24] Pierce, A. D. Acoustics: an introduction to its physical principles and applications. New York: Springer, 2019.
[25] Li, J., Chan, C. T.: Double-negative acoustic metamaterial. Phys Rev E **70**, 55602 (2004) 10.1103/PhysRevE.70.055602.
[26] Forcella, D., Prada, C., Carminati, R.: Causality, Nonlocality, and Negative Refraction. Phys Rev Lett **118**, 134301 (2017) 10.1103/PhysRevLett.118.134301.
[27] Agranovich, V. M., Ginzburg, V. Crystal optics with spatial dispersion, and excitons. Springer Berlin, Heidelberg, 2013.
[28] Chen, Y., Wang, K., Kadic, M., et al: Extraordinary phonon transmission through a nonlocal metamaterial slab. submitted (2022)